

## DEVELOPMENT OF AN AEROSERVOELASTIC MATHEMATICAL MODEL OF A MISSILE CONTROL FIN

Mehmet Ozan Nalci<sup>1</sup>  
Roketsan Missile Industries Inc.  
Ankara, Turkey

Altan Kayran<sup>2</sup>  
Middle East Technical University  
Ankara, Turkey

### ABSTRACT

In this study, the derivation of a mathematical model of a missile control fin aeroservoelastic system, is performed. The structural, aerodynamic and servo-actuation system model parameters obtained in a separate study are implemented to the aeroservoelastic mathematical model, and the aeroservoelastic system is analyzed both in frequency and time domain. To provide genericity, structural mathematical modeling is performed on finite element modeling basis. Aerodynamic mathematical modeling of the missile control fin is based on "Generalized Aerodynamic Force" (GAF) matrix generation, whose values can be obtained by panel discretization based finite element methods or more advanced 3D CFD methods. A rational function approximation formulation of the GAF matrices is presented, in order to be able to represent the aerodynamic forces in the continuous frequency domain. Both the elastic and rigid body motion of the missile control fin are modeled by modal discretization, so that the interaction between the aeroelastic system and the control system dynamics could be studied. The inertial and aerodynamic coupling between the rigid body and elastic motion due to control actuation are formulated. A PD controller is augmented to the aeroservoelastic system, to simulate the behaviour of the overall system in response to various control commands.

### INTRODUCTION

Aeroservoelasticity studies the interaction between aerodynamic, inertial, elastic and control forces that act on an aircraft. The interaction between control dynamics and aeroelastic properties of an aircraft naturally inherits transient dynamics, therefore aeroservoelasticity is a topic of dynamic aeroelasticity. Steady and unsteady effects on the structure are studied, since both interact with control system dynamics. The structure being analyzed may be a single control surface or a full aircraft with control surfaces.

The structural dynamics, aerodynamics and the actuator dynamics have long been represented by linear models, rendering possible the analysis of the aeroservoelastic system in the frequency domain [Karpel, M., 1982]. The structural dynamics of all movable control surfaces with linear structural properties is commonly modeled utilizing the finite element method, putting forward modal discretization to account for both the rigid body and the flexible motion [Karpel, M., and Sheena, Z., 1989]. Together with the finite element formulation of the structural dynamics, the Doublet Lattice Method [Albano, E., and Rodden, W. P., 1969] of aerodynamics has been used for carrying out flutter analysis and obtaining the Generalized Aerodynamic Force (GAF) matrices at discrete reduced frequencies. These GAF matrices are then input to a Rational Function Approximation (RFA) method such as Roger's RFA [Roger, K. L., 1977] to obtain continuous frequency domain representation of aerodynamics over a specified frequency range as a function of the Laplace variable 's'. The inverse Laplace transform of the continuous frequency domain representation renders possible the time domain analysis of the aeroservoelastic system.

---

<sup>1</sup> Senior Modeling and Simulation Engineer in Roketsan Missile Inc., Email: onalci@roketan.com.tr

<sup>2</sup> Professor at the Department of Aerospace Engineering, Email: akayran@metu.edu.tr

The present study presents a generic aeroservoelastic model, that renders possible the important physical phenomena involved in the aeroservoelastic motion to be studied. To provide genericity in structural modeling, the finite element formulation of structural dynamics is utilized. Aerodynamic modeling is handled with intermediate complexity, by utilizing a panel discretization method, The Doublet Lattice Method (DLM) of subsonic flow. The Generalized Aerodynamic Force matrices obtained are fitted for a range of reduced frequencies with Roger's RFA method, so that the pure oscillatory aerodynamic forces can be represented in the time domain. The aerodynamic and structural matrices are integrated, also by accounting for rigid body motion, through a procedure which is well documented by Karpel [Karpel, M., 1990]. The formulation allowed the state space representation of the dynamics of aeroservoelasticity. Frequency domain and time domain analyses are performed with the aeroservoelastic model, in order to deduce the model fidelity achieved. The scope of the analysis is expanded to linear analysis, power limited nonlinear analysis, stability analysis with different feedback paths and performance analysis with regard to performance requirements of the servoactuation system.

## MATHEMATICAL MODELING

### The Aeroelastic Model

In aircraft structural dynamics analysis, modal reduction is usually employed to reduce the problem size. The physical motivation behind the reduction process is that, in general a relatively narrow frequency range of interest dominates the dynamics of the structure. Through a proper selection of a number of low frequency structural modes, it is possible to capture the dominant dynamics of a structure and reduce the problem size. For the cases where an independent external forcing is also involved, the frequency content of the external forcing agents should be taken into account. Equations (1) and (2) represent the equation of motion of the missile control fin with respect to modal coordinates  $\zeta_m$ , in time domain and Laplace domain respectively.

$$[\mathbf{M}_{mm}] \{\ddot{\zeta}_m(t)\} + [\mathbf{C}_{mm}] \{\dot{\zeta}_m(t)\} + [\mathbf{K}_{mm}] \{\zeta_m(t)\} = \{F_m(\zeta_m, \dot{\zeta}_m, \ddot{\zeta}_m, t)\} \quad (1)$$

$$(s^2 [\mathbf{M}_{mm}] + s [\mathbf{C}_{mm}] + [\mathbf{K}_{mm}]) \{\zeta_m(s)\} = \{F_m(s)\} \quad (2)$$

Where  $\mathbf{M}_{mm}$ ,  $\mathbf{C}_{mm}$  and  $\mathbf{K}_{mm}$  are the reduced modal mass, damping and stiffness matrices respectively, and  $F_m(\zeta_m, \dot{\zeta}_m, \ddot{\zeta}_m, t)$  is the vector of external forces at modal coordinates. Equation (2) can be rewritten, by expressing the aeroelastic system at the left hand side, and the external control force applied by the actuator at the right hand side of Equation (3).

$$(s^2 [\mathbf{M}_{mm}] + s [\mathbf{C}_{mm}] + [\mathbf{K}_{mm}] - q[\bar{\mathbf{Q}}_{mm}(M, s)]) \{\zeta_m(s)\} = \{T_{act}(s)\} \quad (3)$$

where  $q$  is the dynamic pressure,  $T_{act}(s)$  is the moment applied by the actuator to the fin and  $\bar{\mathbf{Q}}_{mm}$  is the reduced modal aerodynamic forcing matrix. The modeshape matrix  $\phi_{am}$  is partitioned into rigid body and flexible modal coordinates  $\phi_{am} = [\phi_{ac} \ \phi_{as}]$ , where  $\phi_{ac}$  is the rigid body mode column vector, and  $\phi_{as}$  is the modeshape matrix that includes elastic modeshapes as column vectors. Then Equation (3) is partitioned to obtain Equation (4).

$$\left( s^2 \begin{bmatrix} \mathbf{M}_{cc} & \mathbf{M}_{cs} \\ \mathbf{M}_{sc} & \mathbf{M}_{ss} \end{bmatrix} + s \begin{bmatrix} 0 & 0 \\ 0 & \mathbf{C}_{ss} \end{bmatrix} + \begin{bmatrix} 0 & 0 \\ 0 & \mathbf{K}_{ss} \end{bmatrix} - q \begin{bmatrix} \bar{\mathbf{Q}}_{cc} & \bar{\mathbf{Q}}_{cs} \\ \bar{\mathbf{Q}}_{sc} & \bar{\mathbf{Q}}_{ss} \end{bmatrix} \right) \begin{Bmatrix} \zeta_c(s) \\ \zeta_s(s) \end{Bmatrix} = \begin{Bmatrix} T_{fin}(s) \\ 0 \end{Bmatrix} \quad (4)$$

Equation (4) can be rewritten in two equation sets as follows :

$$(s^2 \mathbf{M}_{cs} - q \bar{\mathbf{Q}}_{cs}) \zeta_s(s) + (s^2 \mathbf{M}_{cc} - q \bar{\mathbf{Q}}_{cc}) \zeta_c(s) = T_{fin}(s) \quad (5)$$

$$\left(s^2\mathbf{M}_{ss} + s\mathbf{C}_{ss} + \mathbf{K}_{ss} - q\bar{\mathbf{Q}}_{ss}\right)\zeta_s(s) + \left(s^2\mathbf{M}_{sc} - q\bar{\mathbf{Q}}_{sc}\right)\zeta_c(s) = 0 \quad (6)$$

In Eqn.(5), the coupling between rigid body dynamics with aeroelastic dynamics is introduced by the inertial and the aerodynamic coupling on  $\zeta_s(s)$ , which is the elastic modal coordinate vector. In Eqn.(6), the coupling between rigid body dynamics with aeroelastic dynamics is introduced by inertial and aerodynamic coupling on  $\zeta_c(s)$ , the rigid body modal coordinate, which is the actuator output  $\theta_{fin}(s)$ . The total hinge moment acting on the transmission unit output shaft, including the aerodynamic and the inertial components is given by Eqn (7).

$$T_{hinge@fin}(s) = -T_{fin}(s) \quad (7)$$

The aerodynamic force matrices in Eqns. (5) and Eqn. (6) are obtained from Roger's RFA utilizing Eqn. (8), where the relation between the reduced frequency and the Laplace variable is taken as  $ik = sb/U$ . In Eqn. (8),  $\mathbf{A}_{0...N+2}$  are the constant matrices to be determined from least square approximation for the best fit of  $\mathbf{Q}(M, s)$ , which is obtained using the DLM. In Eqn. (8),  $\beta_n$  are the aerodynamic lag roots which are preset to specific values in the frequency range of interest, so that the aerodynamic lag functions are stable, the least square problem becomes linear, and the fit is satisfactory.

$$[\bar{\mathbf{Q}}(M, s)] = [\mathbf{A}_0] + \frac{sb}{U}[\mathbf{A}_1] + \left(\frac{sb}{U}\right)^2[\mathbf{A}_2] + \sum_{n=1}^N \frac{s[\mathbf{A}_{n+2}]}{s + \frac{b}{\beta_n}} \quad (8)$$

Aeroelastic matrices given below are defined for subsequent use. In the definition of the aeroelastic matrices, all coefficients  $\mathbf{A}_{0...N+2}$  are obtained from Roger's RFA.

$$\begin{aligned} \bar{\mathbf{M}}_{cs} &= \mathbf{M}_{cs} - \frac{\rho b^2}{2} \mathbf{A}_{cs_2} & \bar{\mathbf{M}}_{cc} &= \mathbf{M}_{cc} - \frac{\rho b^2}{2} \mathbf{A}_{cc_2} & \bar{\mathbf{K}}_{cs} &= -\frac{\rho U^2}{2} \mathbf{A}_{cs_0} & \bar{\mathbf{K}}_{cc} &= -\frac{\rho U^2}{2} \mathbf{A}_{cc_0} \\ \bar{\mathbf{C}}_{cs} &= -\frac{\rho b U}{2} \mathbf{A}_{cs_1} & \bar{\mathbf{C}}_{cc} &= -\frac{\rho b U}{2} \mathbf{A}_{cc_1} & \bar{\mathbf{M}}_{ss} &= \mathbf{M}_{ss} - \frac{\rho b^2}{2} \mathbf{A}_{ss_2} & \bar{\mathbf{M}}_{sc} &= \mathbf{M}_{sc} - \frac{\rho b^2}{2} \mathbf{A}_{sc_2} \\ \bar{\mathbf{C}}_{ss} &= \mathbf{C}_{ss} - \frac{\rho b U}{2} \mathbf{A}_{ss_1} & \bar{\mathbf{C}}_{sc} &= -\frac{\rho b U}{2} \mathbf{A}_{sc_1} & \bar{\mathbf{K}}_{ss} &= \mathbf{K}_{ss} - \frac{\rho U^2}{2} \mathbf{A}_{ss_0} & \bar{\mathbf{K}}_{sc} &= -\frac{\rho U^2}{2} \mathbf{A}_{sc_0} \end{aligned}$$

Two types of aerodynamic lag states are defined so that a state space formulation for the solution of  $\zeta_s(s)$  could be constructed. The aeroelastic hinge moment lag state is given by Eqn. (9), which is used for constructing the hinge moment as an output of the state space aeroelastic system model. The lag state for the aeroelastic equation of motion is given in Eqn. (10).

$$\zeta_{c_{an}}(s) = \frac{s\mathbf{A}_{cs_{n+2}}}{s + \frac{b}{\beta_n}} \zeta_s(s) + \frac{s\mathbf{A}_{cc_{n+2}}}{s + \frac{b}{\beta_n}} \zeta_c(s) \quad (9)$$

$$\zeta_{s_{an}}(s) = \frac{s\mathbf{A}_{ss_{n+2}}}{s + \frac{b}{\beta_n}} \zeta_s(s) + \frac{s\mathbf{A}_{sc_{n+2}}}{s + \frac{b}{\beta_n}} \zeta_c(s) \quad (10)$$

Then, the state space formulation of the aeroelastic system augmented with hinge moment lag states is obtained as in Eqn. (11).

$$\{\dot{z}(t)\} = [\mathbf{A}_{sys}] \{z(t)\} + [\mathbf{B}_{sys}] \{u(t)\} \quad (11)$$

The system and input matrices are expressed as:

$$\begin{aligned}
 [\mathbf{A}_{sys}] &= \begin{bmatrix} 0 & \mathbf{I} & 0 & 0 \\ -\bar{\mathbf{M}}_{ss}^{-1}\bar{\mathbf{K}}_{ss} & -\bar{\mathbf{M}}_{ss}^{-1}\bar{\mathbf{C}}_{ss} & q\bar{\mathbf{M}}_{ss}^{-1}\mathbf{D}_s & 0 \\ 0 & \mathbf{E}_{ss} & \frac{U}{b}\mathbf{R}_{ss} & 0 \\ 0 & \mathbf{E}_{cs} & 0 & \frac{U}{b}\mathbf{R}_{cs} \end{bmatrix} & \{z(t)\} &= \begin{Bmatrix} \zeta_s(t) \\ \dot{\zeta}_s(t) \\ \zeta_{sa1}(t) \\ \dots \\ \zeta_{saN}(t) \\ \zeta_{ca1}(t) \\ \dots \\ \zeta_{caN}(t) \end{Bmatrix} \\
 [\mathbf{B}_{sys}] &= \begin{bmatrix} 0 & \mathbf{I} & 0 \\ \bar{\mathbf{M}}_{ss}^{-1}\bar{\mathbf{K}}_{sc} & \bar{\mathbf{M}}_{ss}^{-1}\bar{\mathbf{C}}_{sc} & -\bar{\mathbf{M}}_{ss}^{-1}\bar{\mathbf{M}}_{sc} \\ 0 & \mathbf{E}_{sc} & 0 \\ 0 & \mathbf{E}_{cc} & 0 \end{bmatrix} & \{u(t)\} &= \begin{Bmatrix} \zeta_c(t) \\ \dot{\zeta}_c(t) \\ \ddot{\zeta}_c(t) \end{Bmatrix}
 \end{aligned}$$

where zeros and  $\mathbf{I}$ 's represent zero and identity matrices,  $z$  is the vector representing the states including the aerodynamic lag states, and  $u$  is the vector representing the control input.

$$\begin{aligned}
 \mathbf{E}_{ss} &= \begin{Bmatrix} \mathbf{A}_{ss3} \\ \mathbf{A}_{ss4} \\ \dots \\ \mathbf{A}_{ssN+2} \end{Bmatrix} & \mathbf{E}_{sc} &= \begin{Bmatrix} \mathbf{A}_{sc3} \\ \mathbf{A}_{sc4} \\ \dots \\ \mathbf{A}_{scN+2} \end{Bmatrix} & \mathbf{R}_{ss} &= \begin{bmatrix} -\beta_1 & 0 & 0 & 0 \\ 0 & -\beta_2 & 0 & 0 \\ 0 & 0 & \dots & 0 \\ 0 & 0 & 0 & -\beta_N \end{bmatrix} \\
 \mathbf{E}_{cs} &= \begin{Bmatrix} \mathbf{A}_{cs3} \\ \mathbf{A}_{cs4} \\ \dots \\ \mathbf{A}_{csN+2} \end{Bmatrix} & \mathbf{E}_{cc} &= \begin{Bmatrix} \mathbf{A}_{cc3} \\ \mathbf{A}_{cc4} \\ \dots \\ \mathbf{A}_{ccN+2} \end{Bmatrix} & \mathbf{R}_{cs} = \mathbf{R}_{ss} &= \begin{bmatrix} -\beta_1 & 0 & 0 & 0 \\ 0 & -\beta_2 & 0 & 0 \\ 0 & 0 & \dots & 0 \\ 0 & 0 & 0 & -\beta_N \end{bmatrix} \\
 \mathbf{D}_s &= [\mathbf{I}_1 \quad \mathbf{I}_2 \quad \dots \quad \mathbf{I}_N]
 \end{aligned}$$

In the relations given above,  $\mathbf{D}_s$  is composed of  $N$  identity matrices of size equal to the number of elastic modal coordinates. The output of the aeroelastic state space system model is formulated, so that the actual displacements at global coordinates, and the hinge moment acting on the fin is calculated. In order to obtain global displacements, modal superposition is used as in Eqn. (12).

$$x(t) = [\phi_{as}] \{\zeta_s(t)\} + [\phi_{ac}] \{\zeta_c(t)\} \quad (12)$$

Hinge moment is expressed in terms of states  $z$  and inputs  $u$  by Eqn.(13)

$$T_{hinge@fin}(s) = T_{hinge@fin}^{state}(s) + T_{hinge@fin}^{input}(s) \quad (13)$$

where

$$T_{hinge@fin}^{state}(s) = (-s^2\bar{\mathbf{M}}_{cs} - s\bar{\mathbf{C}}_{cs} - \bar{\mathbf{K}}_{cs} + q\chi_{cs}^l(s))\zeta_s(s) \quad (14)$$

$$T_{hinge@fin}^{input}(s) = (-s^2\bar{\mathbf{M}}_{cc} - s\bar{\mathbf{C}}_{cc} - \bar{\mathbf{K}}_{cc} + q\chi_{cc}^l(s))\zeta_c(s) \quad (15)$$

where  $cc$ ,  $cs$ ,  $sc$  and  $ss$  sets of  $x^l(s)$  is given by  $x^l(s) = \sum_{n=1}^N \frac{s\mathbf{A}_{n+2}}{s + \frac{U}{b}\beta_n}$ .

Formulating Eqn. (14) and Eqn. (15) in state space form, the hinge moment is formulated as an output in Eqn. (16).

$$T_{hinge@fin}(t) = [\mathbf{C}_{hinge@fin}] \{z(t)\} + [\mathbf{D}_{hinge@fin}] \{u(t)\} \quad (16)$$

The output matrix and the direct transition matrix are defined in Eqn. (17) and Eqn. (18),

$$\mathbf{C}_{hinge@fin} = \begin{bmatrix} -\bar{\mathbf{K}}_{cs} & -\bar{\mathbf{C}}_{cs} & 0 & q\mathbf{D}_c \end{bmatrix} - \bar{\mathbf{M}}_{cs}\bar{\mathbf{M}}_{ss}^{-1} \begin{bmatrix} -\bar{\mathbf{K}}_{ss} & -\bar{\mathbf{C}}_{ss} & q\mathbf{D}_s & 0 \end{bmatrix} \quad (17)$$

$$\mathbf{D}_{hinge@fin} = \begin{bmatrix} -\bar{\mathbf{K}}_{cc} & -\bar{\mathbf{C}}_{cc} & -\bar{\mathbf{M}}_{cc} \end{bmatrix} - \bar{\mathbf{M}}_{cs}\bar{\mathbf{M}}_{ss}^{-1} \begin{bmatrix} \bar{\mathbf{K}}_{sc} & \bar{\mathbf{C}}_{sc} & -\bar{\mathbf{M}}_{sc} \end{bmatrix} \quad (18)$$

where  $\mathbf{D}_c$  is an  $N$  size row vector composed of 1's. Eqn. (11), Eqn. (12) and Eqn. (16) form the state space aeroelastic system model together with its outputs as displacements in global coordinates and total hinge moment around the fin. All the aeroelastic matrices presented in the formulation are obtained by normal modes and flutter analysis carried out in MSC Nastran. Further detail on how the aeroelastic matrices are obtained, is included in [Nalci, O., Kayran, A., 2013].

### The Control System Model

Hydraulic, pneumatic and electromechanical servo actuation systems have distinctive dynamic characteristics, which will make the response of the aeroservoelastic system differ in terms of both stability and performance. An electromechanical servo-actuator system model is integrated to the aeroelastic system in this work, to study the aeroservoelastic dynamics. The electromechanical servo-actuation system is made up of a DC Motor, a transmission unit and a PD Controller. In Figure 1, a generic block diagram of a servo-actuation system is shown.

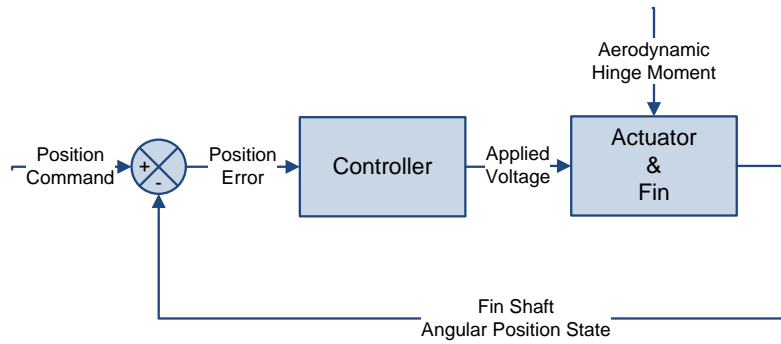


Figure 1 Block Diagram of the Servo-Actuation System

Linear transfer functions for the servo-actuation system are presented in this section. These transfer functions are used for Root Locus [Evans, W. R., 1948] design of the PD controller. Nonlinear parameters such as dry friction and free play in mechanical linkages are neglected. On the other hand, the effect of the power limit nonlinearity of the DC Motor is modeled in MATLAB Simulink.

In aerospace applications, especially in missile system design, the size of the servo-actuation system is constrained by packaging requirements of the missile. These constraints are commonly reflected on the servo-actuation unit by limiting its diameter and length, and the placement in the missile. On the other hand, significant aerodynamic hinge moments on the control surfaces have to be tolerated and the performance of the servo-actuation system should be sustained in a vast range of flight conditions. Therefore a gearbox with a specific speed reduction ratio is commonly used to provide the necessary torque to actuate the fin without performance degradation. In addition, because of the cylindrical shape of the DC Motors used, they are commonly placed in the missile so that the rotational motion of the motor output shaft is parallel to the missile's longitudinal axis, as shown in Figure 2. Therefore

there is a need for transmitting the rotational motion of the motor output shaft onto the axis of rotation of the control surface. A transmission unit with speed reduction is commonly used for this purpose.

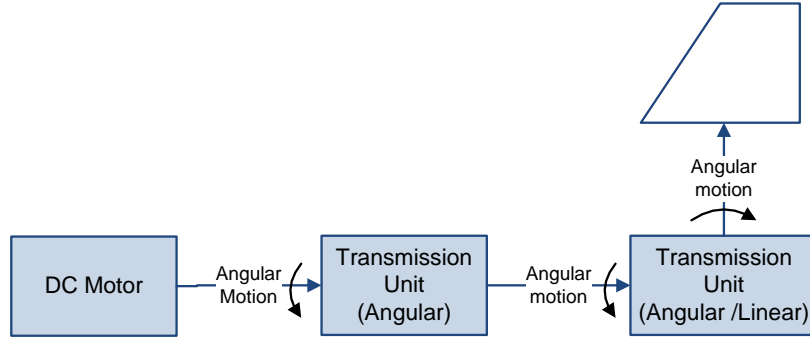


Figure 2 Common Actuator Placement in Missiles

In this study, a combined transmission unit with a specific speed reduction ratio and efficiency is modeled by Eqn. (19) to Eqn. (21):

$$\theta_m = \theta_{fin} N_{tr} \quad (19)$$

$$J_{total @ motor} = J_{rotor} + J_{gear @ motor} + \frac{J_{fin}}{N_{tr}^2 \eta_{tr}} \quad (20)$$

$$T_{hinge @ motor} = \frac{T_{hinge @ fin}}{N_{tr} \eta_{tr}} \quad (21)$$

where the parameters in Eqn. (19) to Eqn. (21) are defined as:

$J_{rotor}$	: Rotor Inertia (kg.m <sup>2</sup> )	$\theta_m$	: Angular Position of Motor Shaft
$J_{gear @ motor}$	: Rotor Inertia (kg.m <sup>2</sup> )	$\theta_{fin}$	: Angular Position of Fin Shaft
$T_{hinge @ motor}$	: Hinge Moment on the Motor (N.m)	$N_{tr}$	: Combined Speed Reduction Ratio
$T_{hinge @ fin}$	: Hinge Moment on the Fin (N.m)	$\eta_{tr}$	: Combined Efficiency

$J_{rotor}$  and  $J_{gear @ motor}$  are obtained from the motor catalog and  $J_{fin}$  is obtained from the MSC PATRAN finite element model.

Dynamic characteristics of a DC Motor are often given in motor catalogs in terms of constant parameters. As long as the DC Motor is used according to the operating conditions that are specified in the catalog such as nominal voltage and max load torque, these parameters are valid for the motor's entire lifecycle. The parameters are listed below:

$V$	: Nominal Voltage (Volts)	$R$	: Armature Resistance (Ohms)
$K_t$	: Torque Constant (N.m/Amperes)	$L$	: Armature Inductance (Henries)
$K_b$	: Back EMF constant (Volts.s/radians)	$c$	: Viscous Damping Coefficient (N.m.s/radians)

When the fin and the transmission units are assumed to be rigid, the output of the transmission unit is equivalent to the output of the fin. Eqn. (22) describes the transfer function between the voltage input of the DC motor and the angular deflection of the fin.

$$\frac{\theta_{fin}(s)}{V_i(s)} = \frac{K_t}{Ns \left( (J_{total @ motor} s + c)(Ls + R) + K_b K_t \right)} \quad (22)$$

When a PD controller is cascaded to the actuator transfer function given in Eqn. (22), a unity feedback closed loop system is formed as shown in Figure 1. Sensor dynamics and error characteristics are neglected, as if the angular position of the fin shaft is perfectly known. Transfer function of a PD controller is given in Eqn. (23).

$$G_{PD}(s) = K_p + K_D s \tag{23}$$

The resulting unity feedback closed loop transfer function is given in Eqn. (24).

$$\frac{\theta_{fin}}{\theta_{com}} = \frac{K_D K_t s + K_p K_t}{N J L s^3 + N (J_{total @ motor} R + c L) s^2 + (N (K_b K_t + c R) + K_t K_D) s + K_p K_t} \tag{24}$$

$\theta_{com}$  is the commanded fin deflection which is equivalent to  $\zeta_c(t)$ .

### AEROSERVOELASTIC MODEL TOPOLOGIES

The mathematical models of servo-actuator and the aeroelastic systems should be integrated, so that the interaction between the control system dynamics and the aeroelastic fin could be studied. By utilizing the MATLAB command 'If' [The MathWorks Inc., 2003] for the generalized feedback interconnection of the actuator and the aeroelastic fin, the linear transfer function of the final aeroservoelastic plant to be controlled is obtained. Figure 3 describes the feedback path for the hinge moment due to inertial and aerodynamic forcing agents.

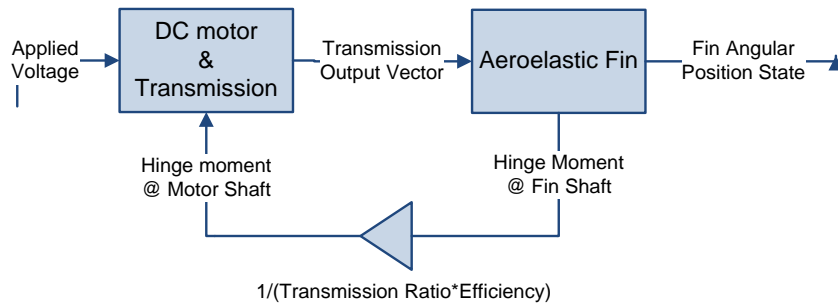


Figure 3 Open Loop Actuator & Aeroelastic Fin System

Two types of aeroservoelastic model topology are used for the frequency and the time domain analysis. The topologies differ in terms of the feedback signal of the controller. Aeroservoelastic Model 1 (AEM1) is assumed to have perfect sensor that measures the motor shaft position. The topology of Aeroservoelastic Model 1 is described in Figure 4.

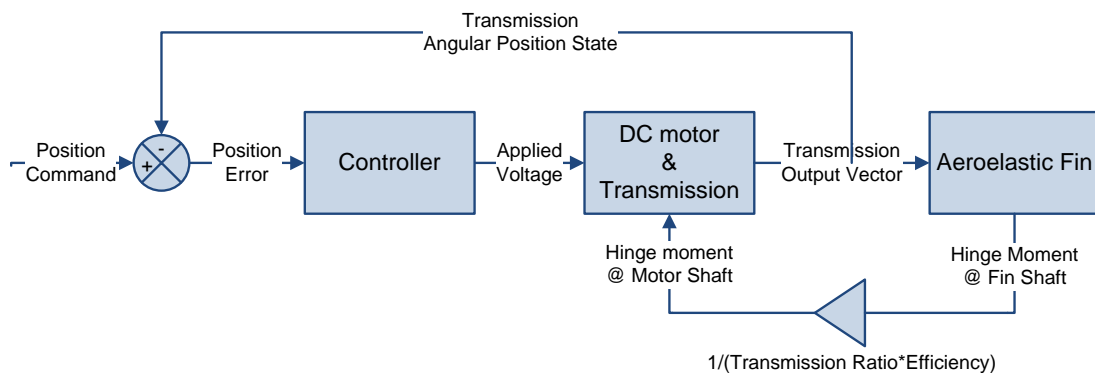


Figure 4 Aeroservoelastic Model 1 (AEM1) Topology

Aeroservoelastic Model 2 (AEM2) is assumed to have a perfect feedback sensor at the fin shaft, that directly measures the angular deflection at the fin root.

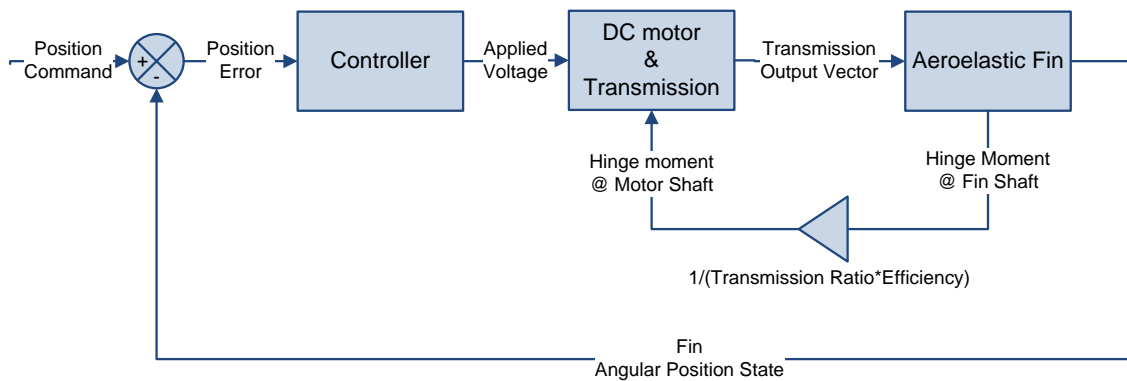


Figure 5 Aeroservoelastic Model 2 (AEM2) Topology

Utilizing the linear models AEM1 and AEM2 time domain and frequency domain analysis could be performed. In addition, the effect of the power limit nonlinearity is introduced by saturating the applied voltage by 24V and the current by 10A. The overall aeroservoelastic system is modeled also in MATLAB Simulink, so that the nonlinearity could be implemented and simulated [Nalçı, O., Kayran, A., 2013].

In order to study the aeroelastic effects with different feedback mechanisms, an initial frequency domain analysis is performed with the forward path transfer functions obtained by cascading the PD controller to three open loop systems; the rigid fin – steady aerodynamics system, AEM1 and AEM2. The forward path transfer functions relate the angular position error to the angular position output of the related feedback mechanism. They are named FWTF1, FWTF2 and FWTF3 respectively. The Bode diagram obtained from the analysis is shown in Figure 6. The linear systems revealed that AEM2 is unstable, since the phase crosses  $-180^\circ$  before the gain falls below 0 dB. Other systems are stable.

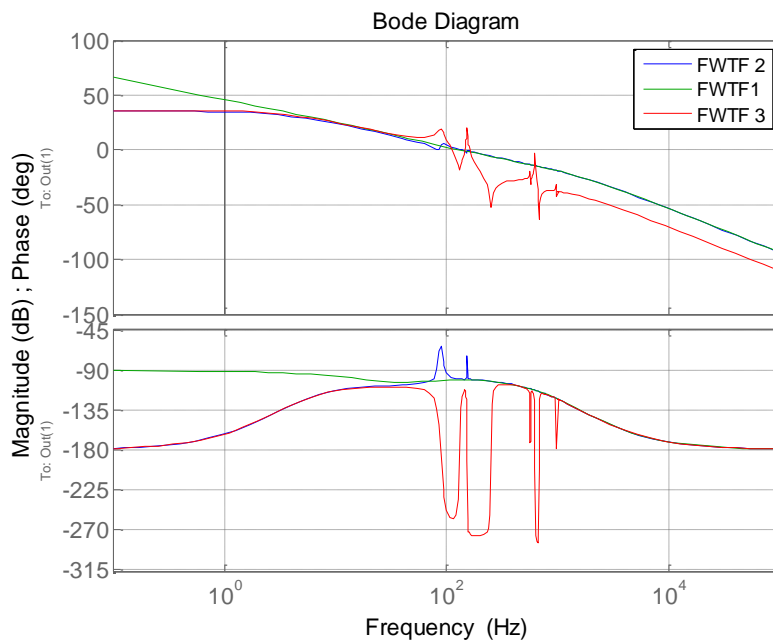


Figure 6 Comparison of Magnitude and Phase Responses of Forward Path Transfer Functions

## NUMERICAL SIMULATIONS OF THE AEROSERVOELASTIC SYSTEM

The parameters in Eqn. (24) were fully obtained in [Nalci, O., Kayran, A., 2013], through the design of a PD controller. The control system design requirements, which are shown to be fulfilled, are restated in Table 1. In order to reveal the interaction between control system dynamics and the aeroelastic fin, linear and power source limited nonlinear time domain simulations are performed with both AEM1 and AEM2. The flutter characteristics were obtained in [Nalci, O., Kayran, A., 2013] by tracking the aeroelastic system root locus, as given in Table 2.

Table 1 Performance Requirements of the Control Fin Response

Settling Time up to 15° Angular Position Command	50 ms
Steady State Angular Position Error	2%
Maximum Load Torque	6 N.m
Minimum Angular Speed at Maximum Load Torque	300°/s

Table 2 Flutter Characteristics at Sea Level

Altitude (m)	0
Mach	0.75
Air Density (kg/m <sup>3</sup> )	1.226
Speed of Sound	340.3
Flutter Point	Aeroelastic Mode 3
Flutter Speed (m/s)	<b>253.11</b>
Flutter Frequency (Hz)	144.1
$U^{eq}$ (m/s)	253.11
$M^{eq}$	0.74

Figure 7 shows the unit step response of AEM1, with and without the effect of power limit, which is specified as 24 V voltage limit and 10 A current limit. According to Figure 7, the nonlinear, power limited response still satisfies the settling time and steady state error requirements given in Table 1. Little oscillation is observed on the transmission output angular position response, which reflects the motor shaft output divided by the combined transmission ratio. Since the linear system behaves faster, there is inevitably an overshoot and more oscillation in the linear response. The transmission output angular position turned out to be satisfactory in terms of the time domain requirements.

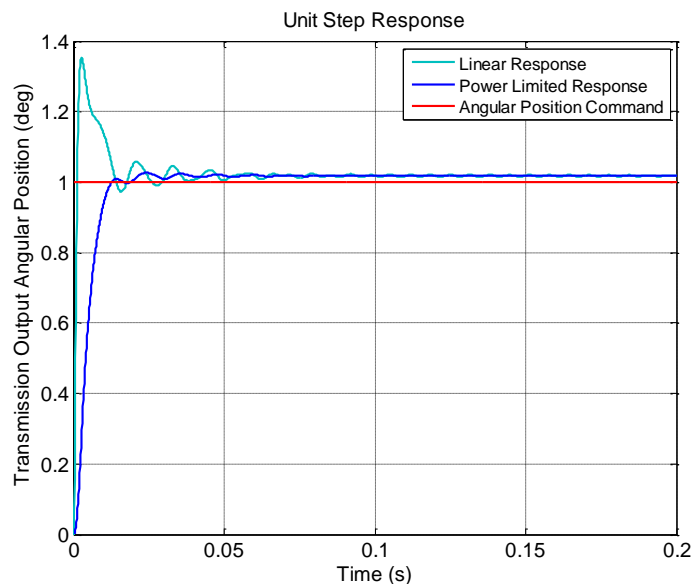


Figure 7 Time History of Transmission Output of AEM1 for Unit Step Input (Linear and Power Limited Nonlinear Models)

In Figure 8, the angular positions at various elastic degrees of freedom are given for a unit step response of AEM1. The lower left corner and the upper right corner are outer corners of the 1<sup>st</sup> and the 42<sup>nd</sup> QUAD4 elements given in Figure 9.

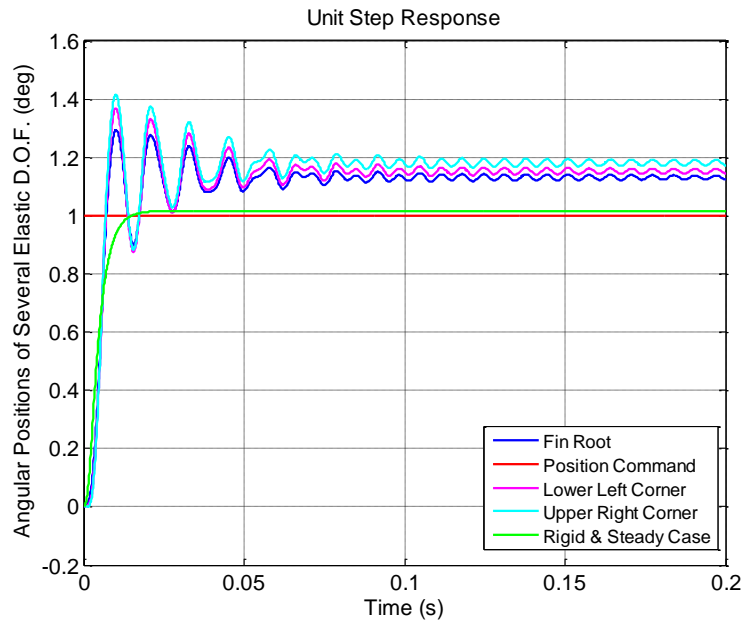


Figure 8 Time History of Various Elastic D.O.F of AEM1 and Rigid Fin for Unit Step Input (Power Limited Nonlinear Model)

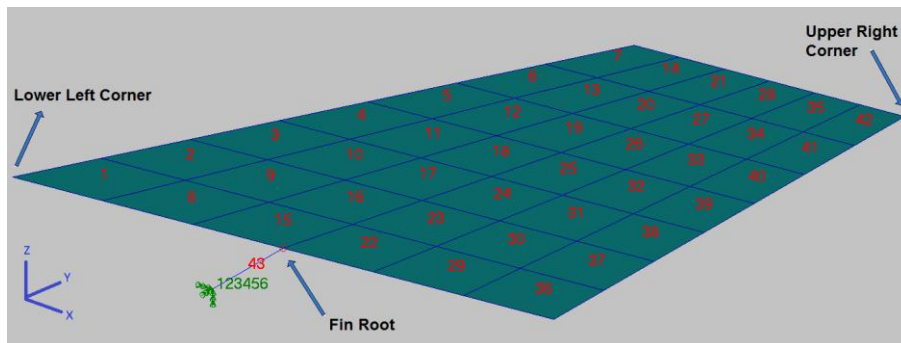


Figure 9 Fin Positions Demonstrated in Figure 8

In Figure 8, it is observed that there is an overshoot of 20% to 40% at different locations on the fin. The response converges to steady oscillation with static elastic deflection amplitude of about 15% of the input. Therefore, it is actually not possible to say that the steady state error requirement is fulfilled when the flexibility of the fin is taken into account. A more qualified approach to this requirement would be to question the total steady lift generated by the control fin at this static elastic deflection, so that the amount of control force provided to the missile could be verified. The green line in Figure 8 is the time history of the servo-actuation system model involving a rigid fin and only steady aerodynamic moment. The deviation of the elastic response from the rigid fin in terms of steady state error and damping behaviour has shown that the fidelity of the rigid fin – steady aerodynamics modeling is unsatisfactory.

The contribution of all five aeroelastic modes to the response can be observed by inspecting the aeroelastic generalized coordinates' time history in Figure 10. Since the first 50 ms of motion is dominated by the transient behavior of the servo-actuation system, the first aeroelastic mode is excited. As a result, its contribution to the oscillatory response is dominant in the transient region. After reaching a steady state value, the oscillatory contribution of the first aeroelastic mode dies out, and

the oscillatory response becomes dominated by the second aeroelastic mode. The oscillations of the second mode dies out rather slower, since this mode is the one at which the flutter is expected. The steady state values of aeroelastic generalized coordinates converging to nonzero values imply the existence of the static elastic deflection.

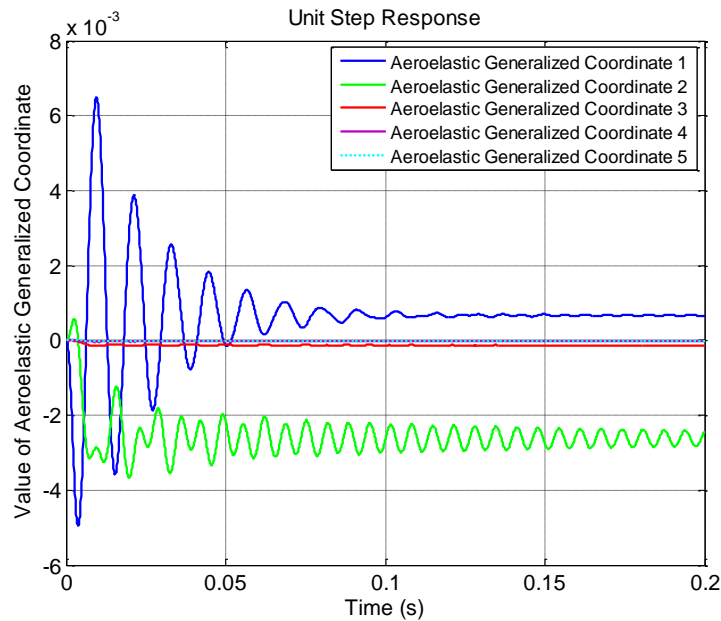


Figure 10 Time History of Aeroelastic Generalized Coordinates of AEM1 for Unit Step Input (Power Limited Nonlinear Model)

The aeroelastic hinge moment history is given in Figure 11, together with the steady aerodynamic moment estimate for the same angular position response. Note that the steady state value of the two hinge moments is different due to elastic static deflection of the fin. The oscillatory nature of the load implies more wear, and more power consumption to compensate for the fluctuations.

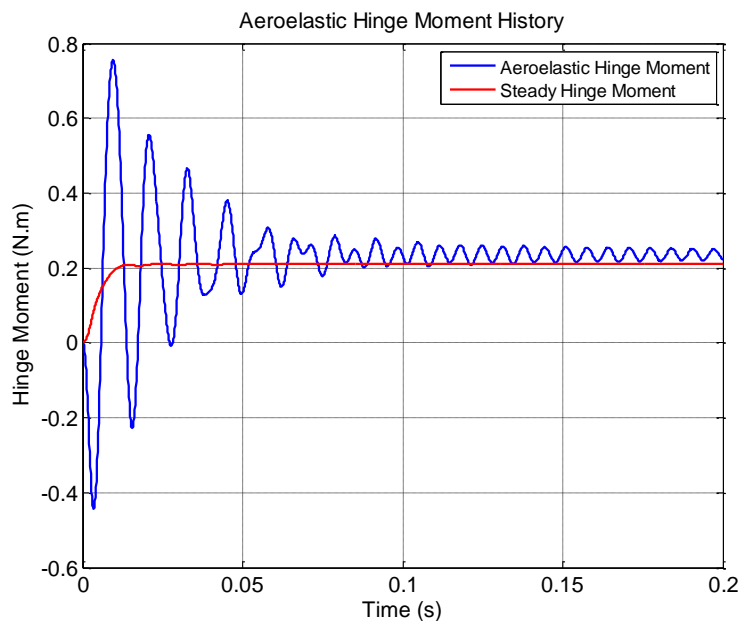


Figure 11 Time History of Hinge Moment of AEM1 for Unit Step Input (Power Limited Nonlinear Model)

The response at the transmission output, to a  $+15^\circ$  step input is simulated and shown in Figure 12, so that the effect of the power limit is fully observed. The nonlinear position response with power limit has very little oscillation and no overshoot, because the system slowed down at higher values of the input

due to increased effect of power saturation. The nonlinearity imposed a desirable effect, reducing overshoot and oscillation, by limiting the bandwidth of the control system.

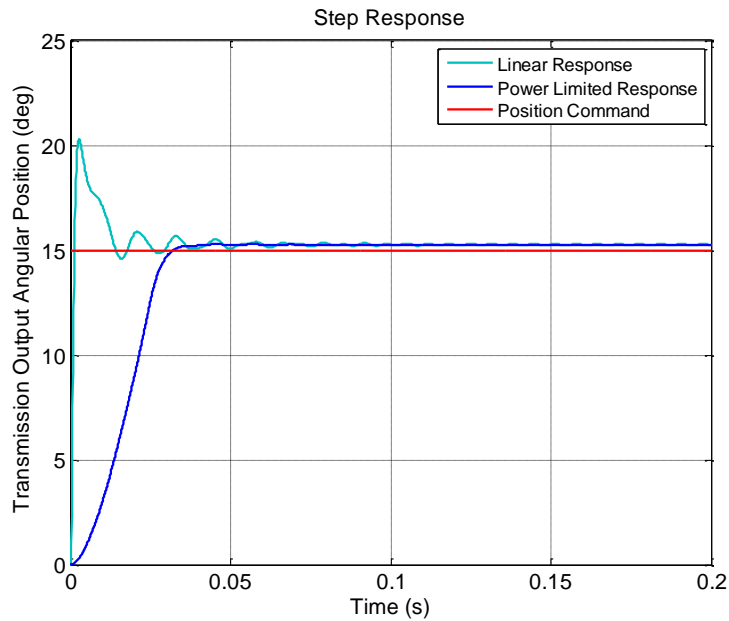


Figure 12 Time History of Transmission Output of AEM1 for  $+15^\circ$  Step Input

The voltage and current time histories are given in Figure 13 and Figure 14 respectively for the unit step input and the  $+15^\circ$  step input. It is observed that the voltage input of the actuator of AEM1 is saturated for a longer time, when the input is  $+15^\circ$ . This input dependency and the limiting nature of the system is inherently nonlinear, but seems to be desirable.

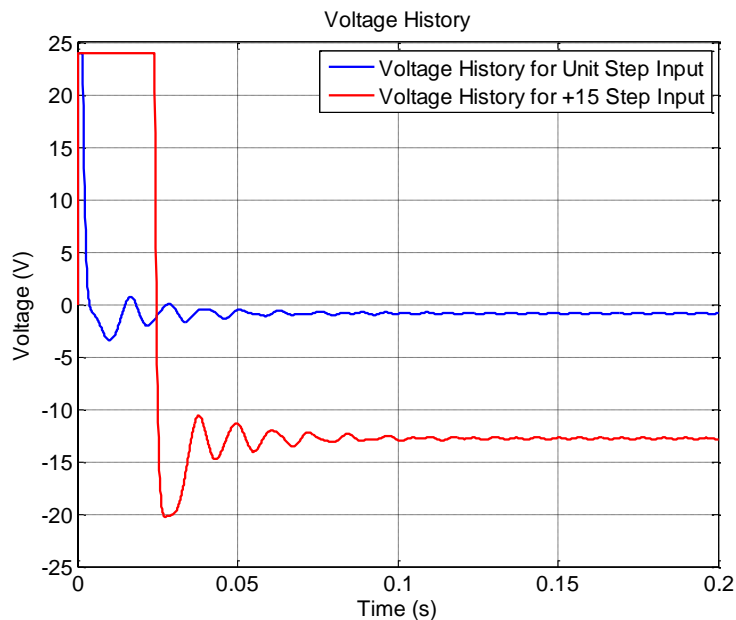


Figure 13 Time History of Voltage Input of AEM1(Power Limited Nonlinear Model)

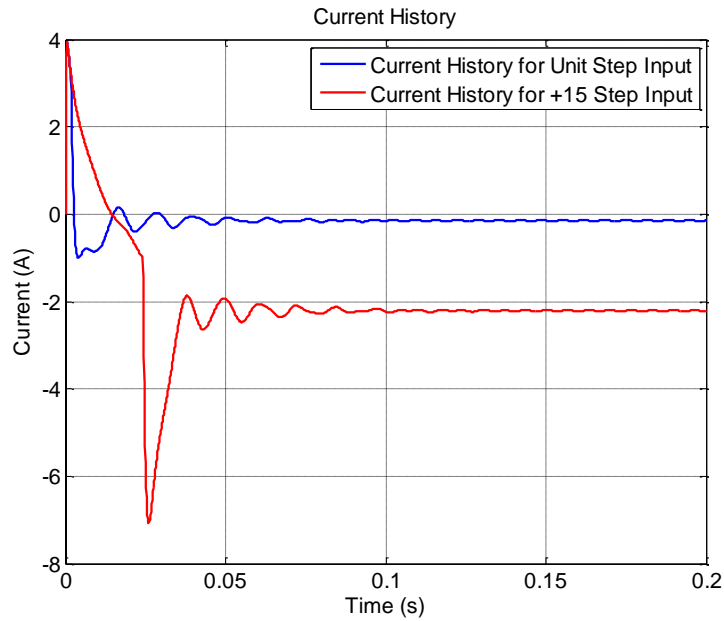


Figure 14 Time History of Voltage Input of AEM1(Power Limited Nonlinear Model)

Figure 15 shows the unit step response of AEM2, without the effect of power limit. According to Figure 15, the linear response is unstable. In this case, because the system is linear, the position response grows unboundedly and AEM2 linear model is dynamically unstable.

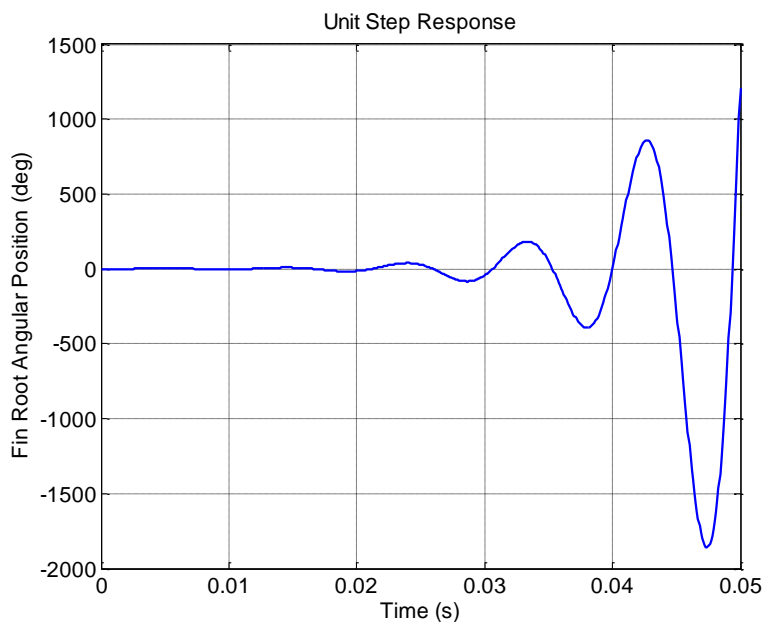


Figure 15 Time History of Fin Root of AEM2 for Unit Step Input (Linear Model)

Figure 16 shows the unit step response of AEM2 with the power limit. The response in this nonlinear case inherits the behavior of many nonlinear unstable systems, namely the limit cycle oscillation. This limit cycle oscillation actually seems to be of desirable type, since it prevents the system from going unstable, but the oscillation amplitude is clearly unacceptable. A nonlinearity may also introduce instability to a system, whereas the linearized version of the system is originally stable. This type of instability may have been observed in AEM1, but the limit on voltage is so high that it did not introduce such effect.

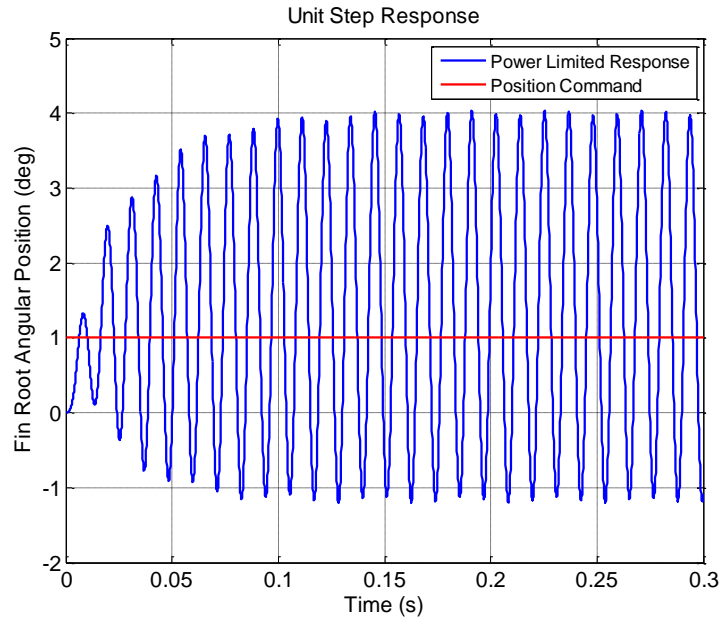


Figure 16 Time History of Fin Root of AEM2 for Unit Step Input (Power Limited Nonlinear Model)

The contribution of all five aeroelastic modes can be observed by inspecting the aeroelastic generalized coordinates' history in Figure 17. The oscillations of the first two aeroelastic modes are sustained, do not grow or decay. The steady state values of aeroelastic generalized coordinates converging to nonzero values imply the existence of the static elastic deflection. In AEM1, second aeroelastic mode was dominant for the steady state response. On the contrary, the first aeroelastic mode seems to be more pronounced than the second aeroelastic mode in AEM2. This is due to the stronger coupling of the servo-actuator dynamics and aeroelastic dynamics in AEM2. Since the first aeroelastic mode's frequency is closer to the servo-actuation system bandwidth than the second aeroelastic mode, it dominates the oscillatory response both for the transient and for the steady state response.

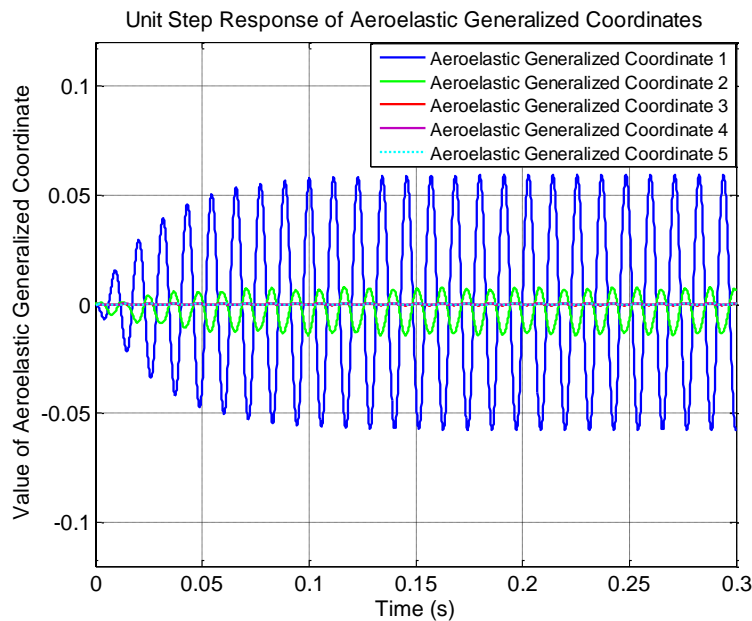


Figure 17 Time History of Aeroelastic Generalized Coordinates of AEM2 for Unit Step Input (Power Limited Nonlinear Model)

## CONCLUSION

In this study, aeroservoelastic modeling and analysis of a missile control surface which is operated and controlled by an electromechanical actuator is performed. The mathematical integration of structural, aerodynamic and servoactuation system models developed on the modal basis is presented. Two distinct aeroservoelastic model topologies are investigated for stability and performance. The models, namely AEM1 and AEM2 are analyzed in frequency domain and time domain, by assuming that the aeroservoelastic system is linear. Moreover, by implementing a power limit nonlinearity, both topologies are analyzed in time domain.

The first model topology having the transmission output position as the feedback signal, named AEM1, turned out to be a stable aeroservoelastic system. The fin's static deflection and oscillatory behavior in AEM1 showed that the fin could not satisfy its 2% steady state error and damped response design requirements. The relation of this undesired response to the governing missile control system and dynamics is emphasized. The second model topology having the fin root position as the feedback signal, named AEM2, responded to input angular position commands with limit cycle oscillations due to the voltage input limit. The oscillation amplitude turned out to be unacceptable. It is observed that the power limited nonlinear models were slower in response; they had lower overshoots and oscillations. The rigid fin – steady aerodynamic loading assumption that lead to the PD controller synthesis is discussed. It is concluded that designing the controller by assuming steady aerodynamic forces and a rigid fin turned out to be unsatisfactory for the fin under study, when the aeroservoelastic phenomena came into the picture.

The resulting aeroservoelastic model is considered to be a generic and fast tool for controller design and aeroservoelastic purposes.

## References

- Karpel, M., "Design for Active Flutter Suppression and Gust Alleviation Using State-Space Aeroelastic Modeling," *Journal of Aircraft*, Vol. 19, No. 3, 1982, pp. 221-227.
- Karpel, M., and Sheena, Z., "Structural Optimization for Aeroelastic Control Effectiveness," *Journal of Aircraft*, Vol. 26, No. 5, 1989, pp. 493-495.
- Albano, E., and Rodden, W. P., "A Doublet Lattice Method for Calculating Lift Distributions on Oscillating Surfaces in Subsonic Flow," *AIAA Journal*, Vol. 7, No. 2, 1969, pp. 279–285.
- Roger, K. L., "Airplane Math Modeling and Active Aeroelastic Control Design," CP-228, AGARD, Brussels, Aug. 1977, pp. 1–11.
- Karpel, M., "Time-Domain Aeroservoelastic Modeling Using Weighted Unsteady Aerodynamic Forces," *Journal of Guidance, Control, and Dynamics*, Vol. 13, No. 1, 1990, pp. 30-37.
- Nalçı, O., Kayran, A, Aeroelastic And Control System Modeling Of A Missile Control Fin For Aeroservoelastic Analysis, 7. ANKARA INTERNATIONAL AEROSPACE CONFERENCE, 11-13 September 2013 - METU, Ankara TURKEY.
- Evans, W. R., "Graphical Analysis of Control Systems," *Transactions of the AIEE*, Vol. 67, 1948, pp. 547–551.
- MATLAB, "User's Manual", Version 6.5, The MathWorks Inc., 2003.MSC.